JOURNAL OF CATALYSIS **158,** 181–192 (1996)
ARTICLE NO. 0017

Electron Microscopy Study of NiW/Al_2O_3-F(x) Sulfided Catalysts Prepared Using Oxisalt and Thiosalt Precursors

J. Ramírez,* P. Castillo,* A. Benitez,* A. Vazquez,† D. Acosta,† and A. López-Agudo‡

*Facultad de Química and †Instituto de Física, Universidad Nacional Autonoma de México, Ciudad Universitaria, Mexico DF, 04510, Mexico; and ‡Instituto de Catálisis y Petroleoquímica, Consejo Superior de Investigaciones Científicas, Campus Universidad Autónoma de Madrid, Cantoblanco 28049, Madrid, Spain

Received June 23, 1994; revised April 11, 1995; accepted September 6, 1995

Two different series of sulfided NiW catalysts supported on alumina modified with different amounts of fluoride, in the range 0.0–2.5 wt%, have been prepared by using two different tungsten precursor salts: ammonium metatungstate and ammonium tetrathiotungstate. Samples of both catalyst series have been examined by the use of high-resolution electron microscopy. For the oxisalt-prepared catalysts the results indicate that fluoride incorporation increases the size of WS_2 crystallites but has little effect on the number of layers. On the other hand, the change of precursor salt significantly influences the stacking of WS_2 crystallites without greatly affecting their size. The thiosalt method of preparation also leads to an excess of sulfur in the catalysts, which is distributed in a nonhomogeneous way.

INTRODUCTION

Conventional hydrodesulfurization (HDS) catalysts, normally cobalt- or nickel-promoted molybdenum or tungsten sulfides supported on alumina, are not particularly effective for high levels of hydrodenitrogenation (HDN) and hydrocracking. When these catalytic functions need to be enhanced, as occurs in the hydroprocessing of heavy petroleum feedstocks, the hydrotreating catalysts must exhibit increased acidity and hydrogenation (HYD) activity. It is known that HDN requires complete saturation of all the aromatic rings prior to any C–N bond cleavage on acid sites (1). Thus, better hydrotreating catalysts could be designed by incorporating an acidic additive like fluoride to NiW/Al_2O_3 catalysts, which are more effective in HYD activity than the $NiMo/Al_2O_3$ catalysts. Fluoride appears in the catalyst formulation of some commercial hydrotreating catalysts.

The effect of fluoride on Mo-based catalysts promoted with nickel has been widely studied (2), but little has been investigated on W-based catalysts. Recently, in an electron microscopy study in which one WS_2/Al_2O_3 sample was examined, it was revealed that the architecture of the WS_2 crystallites in WS_2/Al_2O_3 catalysts behaves quite differently from that of the corresponding MoS_2 crystallites in MoS_2/Al_2O_3 catalysts (3). These differences in behavior are not only due to changes in the nature of the oxometallate entities present in the impregnating solution but also to the fact that polyoxotungstates are more difficult to sulfide than the corresponding oxomolybdates.

Preliminary results of characterization (by X-ray diffraction, diffuse reflectance spectroscopy, Raman spectroscopy, temperature-programmed reduction, and acidity measurements) of tungsta supported on fluorinated alumina (4) showed that fluoride incorporation favored the formation of polytungstates and increased the reducibility of tungsten species. The catalytic activity results (5) showed that both HDS and HDN activities clearly increased with fluoride loading, the increase being relatively larger for HDN than for HDS.

Additional characterization by high-resolution electron microscopy of the sulfided W catalysts (5) revealed that the incorporation of fluoride contents of 1.5 wt% promoted a better sulfidation of the WO_3 precursor. In a recent communication (6), it was suggested from high-resolution transmission electron microscopy and temperature-programmed sulfidation that fluoride addition to a NiW/Al_2O_3 catalyst increased the metal dispersion and the reaction rates for thiophene HDS and *n*-heptane hydroprocessing. Our results on sulfided NiW/Al_2O_3–F(x) catalysts indicate, however, that fluoride incorporation only slightly affects the activity for thiophene HDS and significantly enhances *n*-heptane hydroconversion (7). Clearly, a greater effort on the characterization of the NiW/Al_2O_3–F system is needed in order to understand the effect of fluoride addition on the surface structure of the sulfided active phase.

Electron microscopy is a helpful technique for obtaining evidence of changes in the morphology, dispersion, and homogeneity of supported metal sulfides. However, in the interpretation of the results one must be aware of the

0021-9517/96 $12.00

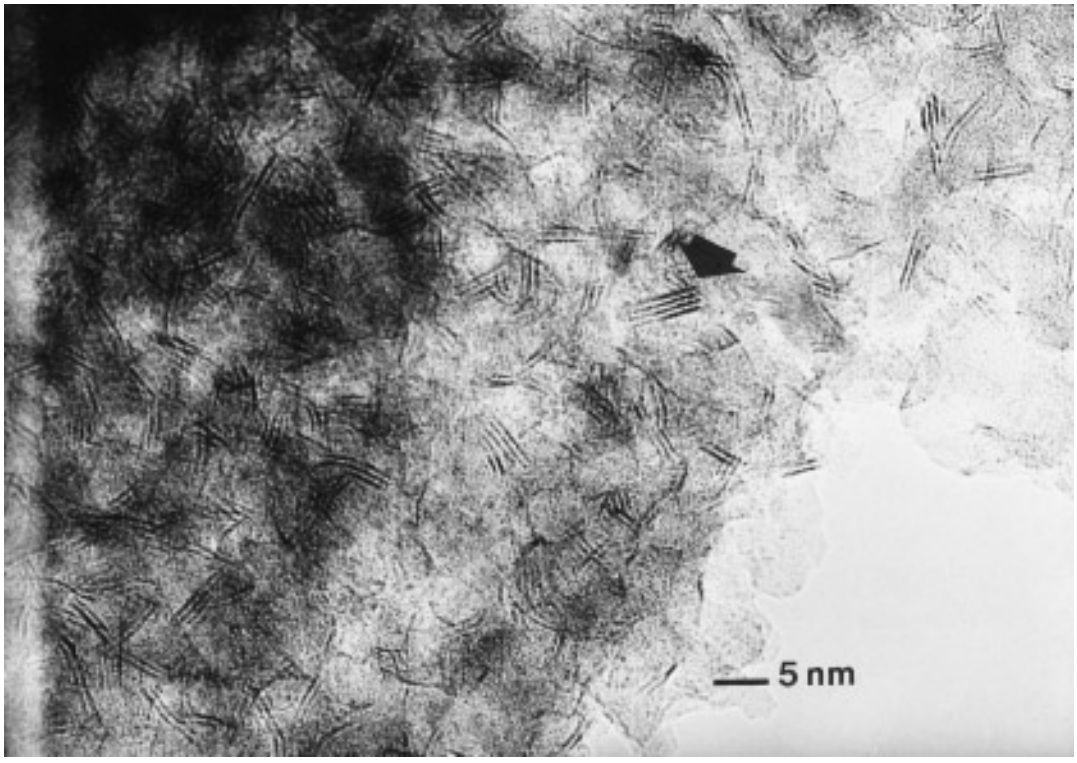

FIG. 1. Micrograph of O–NiW–F(1.5) sulfided catalyst showing the typical WS_2 slabs with interplanar distances of about 6.18 Å.

limitations of the technique. Clearly, one of the limits comes from the difficulty in observing very small WS_2 particles of less than 1 nm. Another limitation of the technique is that during the observations, only the WS_2 platelets which have the *c* axis perpendicular to the incident beam would be imaged. This last point would be of importance when catalysts supported on very different supports are being compared. In our case where there are only small changes in surface area, texture, and structure of the alumina support, and more than 300 particles were measured in each sample, the above difficulties are probably of minor importance. Thus, in this work we present the observations of an electron microscopy study of sulfided NiW/Al_2O_3 catalysts containing different amounts of fluoride incorporated into the alumina support, prepared by conventional impregnation with ammonium metatungstate. A similar series of catalysts prepared by impregnation with a tungsten thiosalt, $(NH_4)_2WS_4$, was also examined. The aim in the latter catalyst series was to observe the effect of this precursor on the morphology and the dispersion of the sulfided phase. The important fact is that using this last precursor, which already has the tungsten in a sulfur environment, eliminates the high-temperature calcination step in which metal oxide–support interaction is promoted, and therefore, a different architecture of the WS_2 crystallites will be possible. The thiosalt precursor has four sulfur atoms in interaction with each W^{6+} ion and therefore it is quite possible that, as a result of the transformation of the ammonium tetrathiotungstate to tungsten disulfide, some excess sulfur will remain in the sulfided catalyst.

EXPERIMENTAL

Catalyst Preparation

Two different series of NiW catalysts, supported on γ-alumina powder (Girdler T-126; Sg = 190 m^2/g, particle diameter equal to 150 mesh) loaded with different amounts of fluoride (0, 0.2, 0.8, 1.5, and 2.5 wt% F^-), were prepared using two different tungsten precursor salts: $(NH_4)_6H_2W_{12}O_{40}$ and $(NH_4)_2WS_4$. In both series, nickel and tungsten were deposited simultaneously by pore volume impregnation of the F-modified alumina with aqueous solutions of nickel nitrate and ammonium metatungstate or ammonium thiotungstate. Surface areas for the fluorinated supports oscillated between 190 m^2/g for the fluoride-free sample and 177 m^2/g for the support with 2.0 wt% F^-. The catalyst series prepared with the tungsten oxisalt, denoted hereafter as O–NiW–F(*x*), where *x* is the wt% F^- content, had a constant content of 20.9 wt% WO_3 (3.8 W atoms/nm^2) and 3.17 wt% NiO equivalent to an atomic ratio Ni/(Ni + W) = 0.32. The impregnated oxisalt samples were dried at 383 K for 2 h and calcined at 823 K for 4.5 h. Sulfidation of these catalysts was carried out at 673 K with a 10 vol% H_2S/H_2 mixture (flow rate, 20 ml/min) for 4 h.

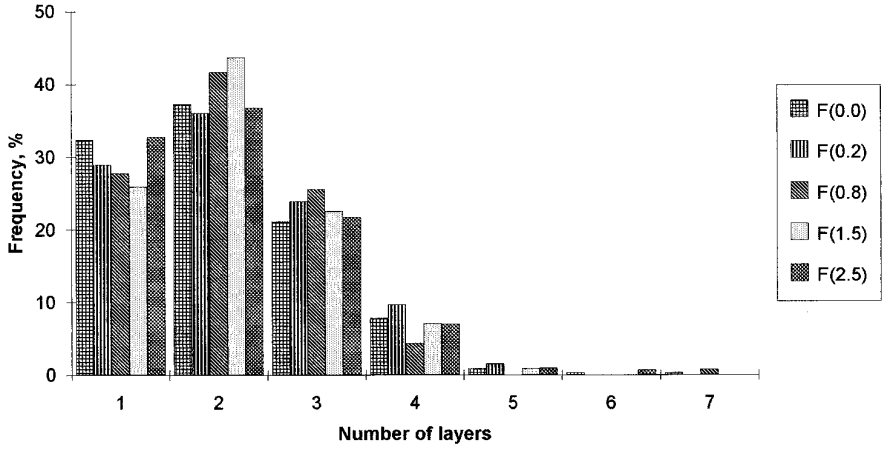

FIG. 2. Distribution plot of the number of layers in the O–NiW–F(x) catalysts.

The catalyst series prepared with thiosalt, denoted hereafter as T–NiW–F(x), had a surface concentration of 2.8 W atoms/nm^2 and an atomic ratio Ni/(Ni + W) = 0.3. The impregnated thiosalt samples were dried at 307 K and decomposed at 400 K in a flow of a 10 vol% H_2S/H_2 mixture (flow rate, 20 ml/min.).

Electron Microscopy

For scanning electron microscopy (SEM) observations, freshly sulfided samples without mechanical treatment were mounted on holders and covered with a gold-sputtered layer and then observed in a Jeol SEM-5200 electron microscope at 25 kV. For conventional transmission electron microscopy (CTEM) and high-resolution electron microscopy (HREM) observations, freshly sulfided samples were placed in an agate mortar half-filled with *n*-heptanol, ground, and dispersed in an ultrasound bath for several minutes. Some drops of the supernatant liquid were then deposited on 200-mesh copper grids previously covered with a holey carbon film. CTEM observations were carried out in a side entrance Jeol 100-CX electron microscope equipped with a Kevex instrument for X-ray analysis. Several bright and dark field images and selected area electron diffraction patterns (SAEDP) were obtained from each sample. HREM observations were carried out in a Jeol 4000-EX electron microscope with 1.7-Å point to point resolution, equipped with a pole piece with a spherical aberration coefficient of Cs = 1.00 mm. Before the samples were transferred from the sulfiding reactor to the microscope they were flushed with nitrogen to eliminate adsorbed H_2S. Transfer of the sulfided samples and their deposition on carbon grids were done under an argon atmosphere. Also, transportation of the grids and their manipulation before being placed in the microscope sample holder were done under an argon atmosphere to avoid contact with air as much as possible.

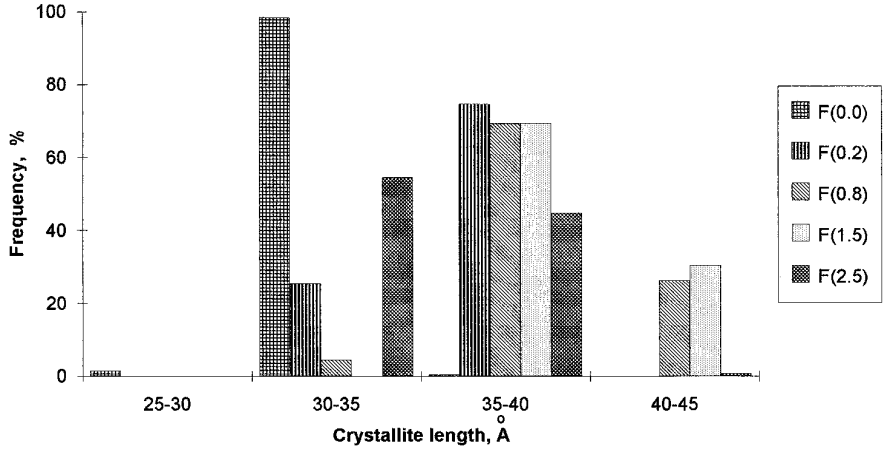

FIG. 3. Crystallite size distribution for the O–NiW–F(x) catalysts.

TABLE 1

Average *N* and *L* Values and Total Observed W Atoms per Square Nanometer, for the Oxisalt-Prepared NiW/Al_2O_3-F(*x*) Catalysts

Fluoride content	N	σ_N[a]	L (nm)	σ_L[a]	Total observed W atoms/nm^2
0	2.09	0.12	3.14	0.10	1.75
0.2	2.19	0.19	3.49	0.16	1.87
0.8	2.10	0.12	3.91	0.07	1.35
1.5	2.13	0.17	3.94	0.18	2.81
2.5	2.09	0.10	3.69	0.14	2.71

[a] Standard deviation for number of layers (σ_N) and crystallite length (σ_L).

For analytical electron microscopy (AEM) studies, fresh samples were mounted in thin graphite bars in order to minimize the effect of spurious signals. All the samples were transported under vacuum in a polycarbonate desiccator to the microscopes, and in all the steps of the preparations contact with air was avoided as much as possible by carrying out the manipulations under an argon atmosphere.

RESULTS AND DISCUSSION

Oxisalt-Prepared NiW/Al_2O_3-F(x) Catalysts

HREM. The micrographs of the O–NiW–F(*x*) catalysts showed clearly (Fig. 1) the typical lattice fringes representing the basal plane of WS_2 structures with 6.18-Å interplanar distances (8, 9). These structures appeared well dispersed in all the samples; however, changes in the stacking and length, depending on the amount of fluoride, were observed.

The number and length of the WS_2 structures of several hundred particles were measured on enlarged micrographs taken from all the samples. Figures 2 and 3 show the percent distribution curves for the number of layers (N) and length of crystallites (L), respectively, of the WS_2 structures in the O–NiW–F(*x*) catalyst series.

Although Fig. 2 shows that in all the catalysts the predominant number of layers is 2, careful examination of the results shows that the incorporation of F^- modified the relative distribution of the number of layers in the catalyst. Thus, the incorporation of F^- into the catalyst, up to F^- contents of 1.5 wt%, produced a decrease in the number of single-layer WS_2 structures and, consequently, an increase in the number of structures with 2 and 3 layers. However, for the catalysts with 2.5 wt% F^-, a number of layers similar to that in the fluoride-free catalyst was found.

Regarding the length of the crystallites, Fig. 3 shows that the fluoride-free catalyst had mostly WS_2 crystallites with lengths between 30 and 35 Å, and a very small proportion of longer crystallites. For the 0.8 and 1.5 wt% F^--containing catalysts, most of the crystallites (70%) were between 35 and 40 Å, and only 25–30% of them presented lengths between 40 and 45 Å. As was the case for the number of layers, the 2.5 wt% F^--containing catalyst did not follow the same trend as the rest of the series; in this case, 55% of the crystallites showed lengths between 30 and 35 Å, and 45% of the crystallites had lengths between 35 and 40 Å.

Table 1 presents the average L and N values for the catalysts with different F^- loadings. From this table it is possible to see that the average stacking of the various formulations was almost constant whereas the average length increased slightly.

An additional feature observed in the micrographs of the catalysts with higher fluoride contents was the presence of patches of well-crystallized alumina (see Fig. 1d). This well-crystallized alumina could be produced by a process of partial solubilization, induced by the fluoride attack and the subsequent recrystallization of the surface alumina during the drying and calcination steps, as previously suggested (5, 10, 11). The recrystallization process may thus generate a surface alumina layer resembling that on the fluoride-free alumina. This process could well be responsible for the similarity between the WS_2 structures found in the catalyst samples with 2.5 and 0.0 wt% fluoride contents.

Thus, in the case of the O–NiW–F(*x*) catalysts, incorporation of fluroide, up to contents of 1.5 wt%, seems to enhance the growth of the crystallites in the lateral direction and induce a slightly higher stacking of the WS_2 structures. Higher fluoride contents (2.5 wt%) seem to invert this trend. The growth of the crystallites in both lateral and vertical directions suggested the possibility of a better sulfidation of the samples, possibly due to a diminished interaction with the alumina support. Since only sulfided crystallites are observed in the HREM micrographs, an increased sulfidation of the samples would lead to a greater density of the WS_2 observed structures. Although by HREM measurements it is not possible to calculate the real degree of sulfidation, since as was mentioned before only the WS_2 platelets with the *c* axis perpendicular to the beam would be imaged, it is possible to estimate a relative degree of sulfidation by calculating for each of the samples the number of observed sulfided tungsten atoms per square nanometer, in all the micrographs taken from each sample. The number of sulfided tungsten atoms observed can be estimated by means of the geometrical model proposed by Kasztelan *et al.* (12). The small WS_2 slabs can be modeled with different geometrical shapes (triangle, rhombus, hexagon), but taking into account the Gibbs–Curie–Wulf law, Toulhoat and Kasztelan (13) have shown that the hexagonal slabs are the most stable of the various possible shapes. Assuming that the average WS_2 crystallite length

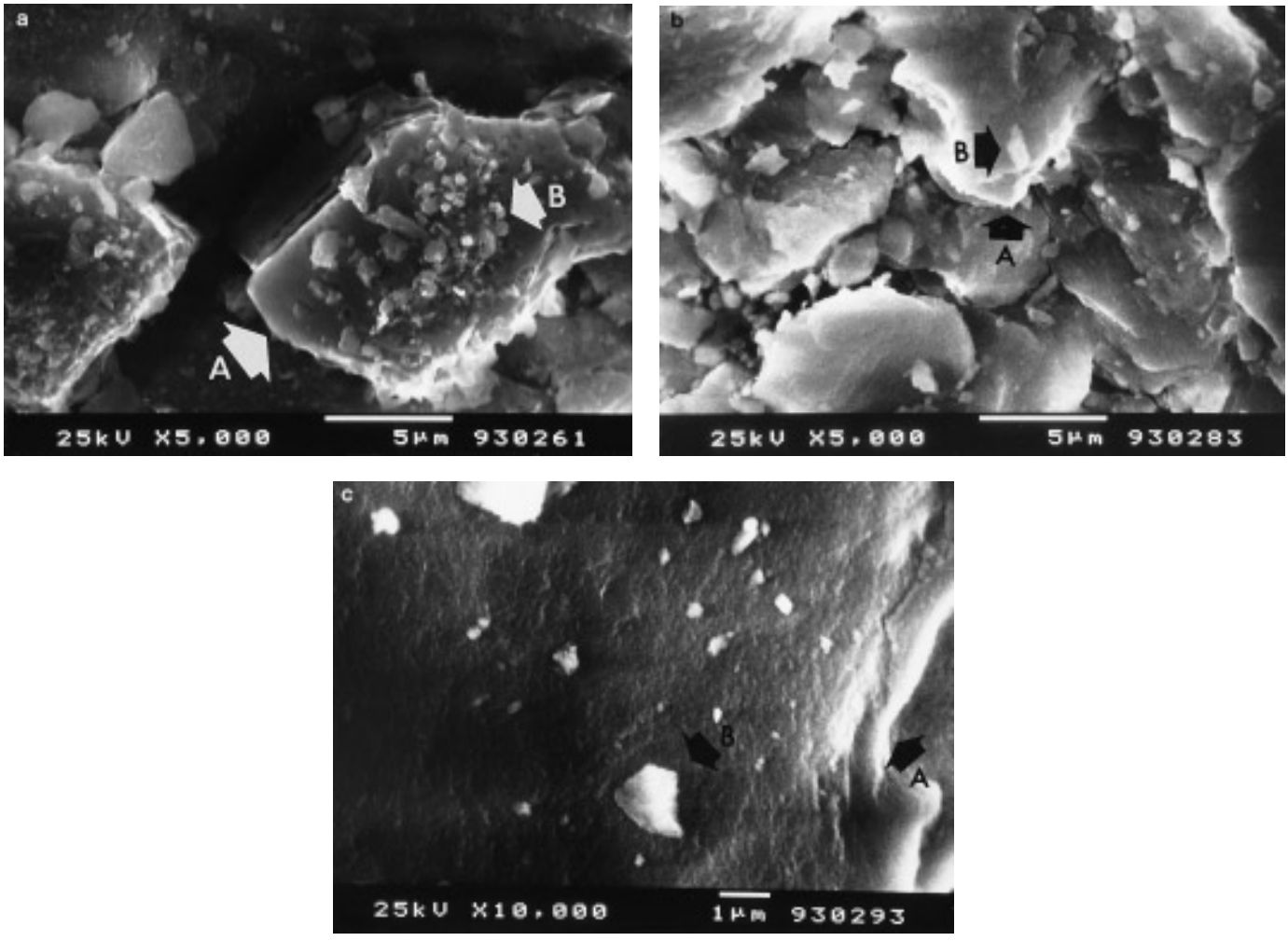

FIG. 4. SEM micrographs of T–NiW–F(x) catalysts showing alumina crystallites of about 10–15 μm (A), and particles of a supported phase (B) of about 1 μm. (a) T–NiW–F(0.0); (b) T–NiW–F(0.2); (c) T–NiW–F(2.5).

(L), determined from HREM measurements, is the longest dimension of the hexagonal crystallites, the total number of tungsten atoms (W_t) can be calculated. This value can be expressed in terms of the number of W–W bonds (n) at the edge of the crystallites, n being equal to one for the entity with seven tungsten atoms. These values can be expressed as

$$W_t = 3n^2 + 3n + 1.$$

Moreover, the length of the slab (L) is related to the number of W–W bonds (n) by

$$L = 2n \times 3.15,$$

where 3.15 is the distance W–W expressed in angstroms. Therefore, with the length of the crystallites obtained by HREM it is possible to calculate n and with this value calculate the total observed tungsten atoms per layer in the WS_2 and since the number of layers of each observer crystallite is also obtained from the HREM micrographs, it is possible to estimate the total number of tungsten atoms per square nanometer observed for each of the catalyst samples. The results from this exercise, for the samples with different contents of fluoride, are shown in Table 1, where it can be observed that indeed the addition of fluoride to the catalysts increases the number of observed tungsten atoms forming part of the WS_2 structures. This result has been interpreted as being due to a better sulfidation of the catalysts when the fluoride loading is increased. Furthermore, since the catalysts were prepared with a tungsten loading of ~3.8 W atoms per square nanometer, it is also evident from the results of Table 1 that although the number of observed tungsten atoms in sulfided form increases with fluoride loading, the level of sulfidation of the most sulfided sample is far from complete and that the

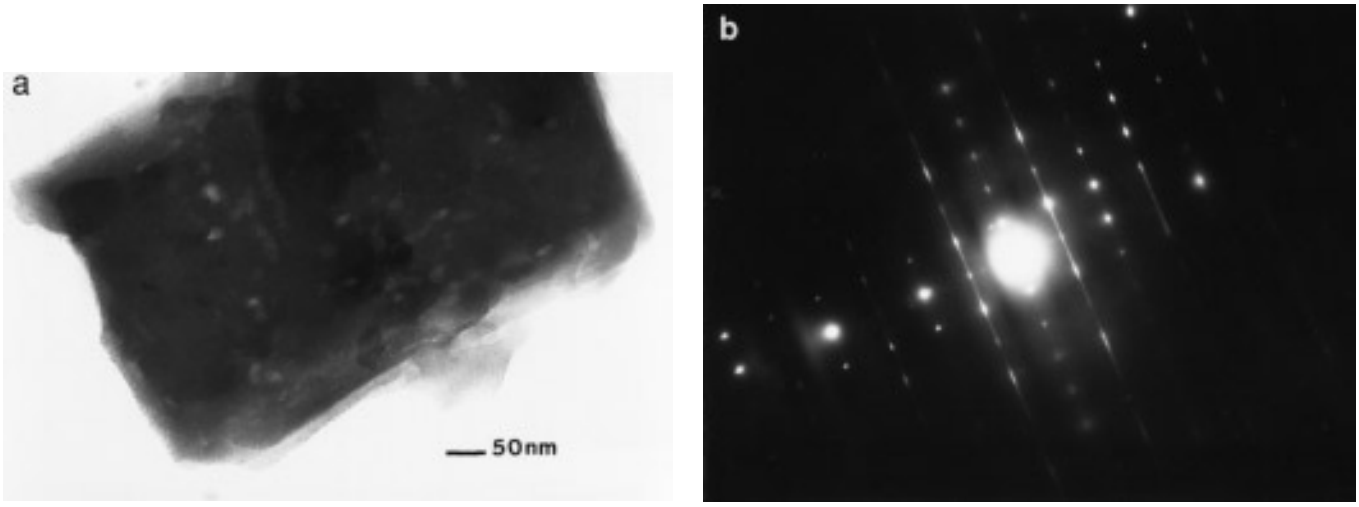

FIG. 5. (a) Crystallite of $(NH_4)_2WS_4$ found in the T–NiW–F(0.0) catalysts. (b) Diffraction pattern of the $(NH_4)_2WS_4$ crystallite, indicating a long crystallite with irregular stacking of layers in a layered compound.

level of sulfidation of the fluoride-free catalyst is quite poor. The difficulty in sulfiding alumina-supported catalyst samples has been reported in the past (14, 15).

Thiosalt-Prepared NiW/Al_2O_3–F(x) Catalysts

Due to the interesting structural features exhibited by this catalyst series, it was studied with scanning electron microscopy, conventional transmission electron microscopy, and high-resolution electron microscopy.

SEM. Figures 4a to 4c present the SEM micrographs of the T–NiW–F(x) catalysts with different F^- contents (0.0, 0.8, and 2.5 wt%). Examination of the micrographs of the fluoride-free catalyst showed the presence of alumina crystals of about 10–15 μm, on top of which grains of a supported phase, of about 1 μm or less, were deposited. The grains of this supported phase, whose nature could not be clearly identified, remained at about the same size when fluoride was incorporated into the catalyst, but their population diminished. Furthermore, the alumina crystals in the fluoride-free sample were well faceted, whereas in the fluoride-containing samples the edges of the alumina crystals appeared smoothed, giving an indication of fluoride attack on the alumina surface.

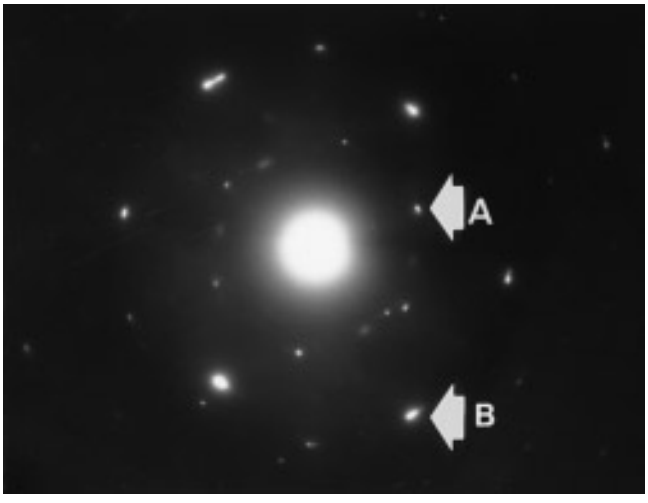

FIG. 6. Diffraction pattern of WS_2 phase found in the T–NiW–F(x) catalysts showing the typical hexagonal arrangement, diffuse dots (A), and some bright dots (B), corresponding to a different nonidentified lattice.

In order to examine the homogeneity of the samples, EDX analysis was performed at two levels of enlargement. The first analysis, called local, was made on areas with the size of one of the supported grains referred to before in the SEM observations (areas of about 1 μm^2). The second analysis, called global, was made on a larger area which encompassed around five of the larger grains which appeared in the SEM photographs (areas around 25 μm^2). The EDX analysis of Al, S, Ni, and W was performed on samples with 0.0, 0.8, and 2.5 wt% F^-. From the results of various local analyses, it was found that the ratio Ni/(Ni + W) varied between 0.209 and 0.49, which when compared to the 0.3 nominal chemical value, indicated the heterogeneity of the system. Also, in general, a great excess of S was found in all the samples. The ratio S/(W + Ni) varied between 3.91 and 4.29 for the global analysis, but for the point to point local analysis it varied from 3.63 to 13.45, confirming the great heterogeneity of the sample. The great excess of sulfur found in several places in the sample was in line with the presence on the catalysts of a tree-like phase, which was identified later as being mainly sulfur (see below).

CTEM. Conventional transmission electron microscopy and selected area electron diffraction patterns of the

FIG. 7. Typical micrograph of T–NiW–F(x) catalysts showing a tree-like phase (A) and another phase (B) which resembles $(NH_4)_2WS_4$ crystallites attached to phase (A).

T–NiW–F(x) samples revealed the presence of various phases in these catalysts.

In the fluoride-free catalyst, several crystals of $(NH_4)_2WS_4$ were detected in addition to the WS_2 phase and the tree-like phase, both of which were present in all the T–NiW–F(x) catalyst samples. Figure 5a shows one of the crystals of $(NH_4)_2WS_4$ found in the 0.0 wt% F^--containing sample. The diffraction pattern of this crystal, shown in Fig. 5b, indicated irregular stacking of layers in a layered compound. Figure 6 shows one of the diffraction patterns obtained of the WS_2 structures, where one can see the well-sulfided WS_2 phase, clearly identified by the

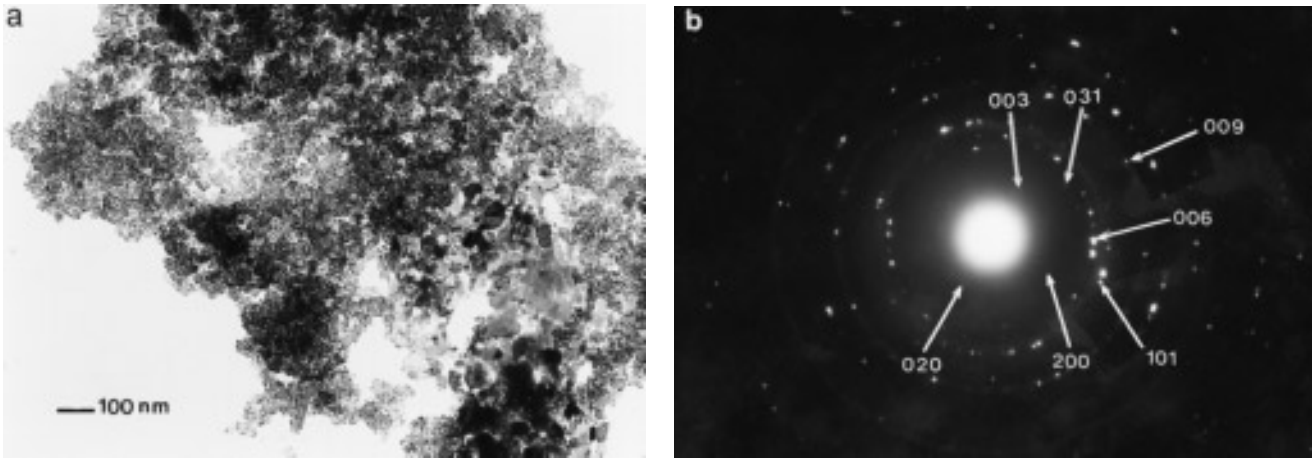

FIG. 8. (a) Bright field micrograph of the T–NiW–F(0.8) catalyst. (b) Diffraction pattern of the whole zone showing the presence of microcrystalline WS_2 [planes (003), (006), (101), (009)], and some weak spots attributed to $(NH_4)_2WS_4$ [planes (020), (200), (031)].

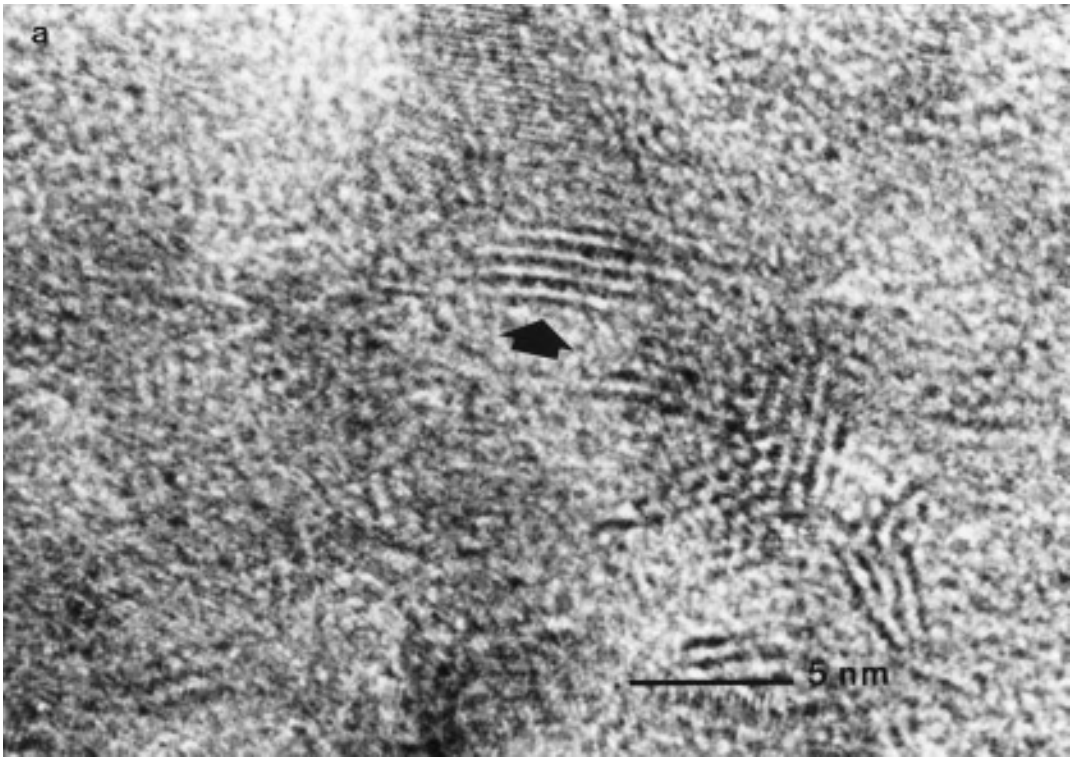

FIG. 9. HREM micrograph of (a) T–NiW–F(0.0), (b) T–NiW–F(0.8), and (c) T–NiW–F(2.5) catalysts showing the stacking and size of WS_2 crystallites.

hexagonal arrangement of diffuse dots (A), in addition to some bright dots (B) which correspond to a different lattice, but which did not show a clear arrangement. Therefore, little can be said about the compound that generates such bright dots.

The tree-like phase (marked A) is shown in Fig. 7, where a second nonidentified phase (denoted B) also appears, which resembles crystals of $(NH_4)_2WS_4$ attached to some of the branches of the tree-like phase. The size of the tree-like phase structures was more than 15,000 nm whereas the faceted B phase attached to some of the branches was about 10 times smaller. SAEDP of the tree-like phases indicated that this phase mainly consisted of sulfur and WS_2. This result was in agreement with the SEM–EDX findings.

The catalysts with incorporated fluoride showed, in general, the same features as the fluoride-free catalysts; however, no crystals of $(NH_4)_2WS_4$ were found in these fluoride-modified catalyst samples, suggesting that fluoride incorporation favored the decomposition of the large thiosalt crystals. To illustrate the features of the fluoride-containing catalysts, Fig. 8a shows a bright-field micrograph of the 0.8 wt% F^--containing catalyst and Fig. 8b shows the diffraction pattern of the whole zone. This diffraction pattern shows the characteristic rings of a polycrystalline material. The interplanar distances derived from this pattern are in agreement with those reported for WS_2 (ASTM card No. 35-651). Also, in the same pattern some weak spots which appeared close to the transmitted beam spot can be assigned to $(NH_4)_2WS_4$ (ASTM card No. 16-213).

HREM. The high-resolution electron micrographs of the T–NiW–F(x) catalysts (x = 0.0, 0.8, and 25 wt%) are shown in Figs. 9a to 9c. In these figures the characteristic lattice fringes representing the basal planes of WS_2 are clearly observed. The WS_2 crystallites appeared well sulfided, in line with the excess of sulfur detected by EDX. However, the WS_2 structures appeared with a higher stacking than in the catalysts prepared by the oxisalt method. Even in the fluoride-free sample, structures with up to eight layers of WS_2 were detected. The number of visible WS_2 structures seemed to increase with the fluoride content, suggesting a better sulfidation.

With respect to the size and stacking, Figs. 10 and 11 show, respectively, the distributions of length and number of layers of the WS_2 crystallites. It can be seen that by increasing the fluoride content, the size of the crystallites increased. The fluoride-free sample had 27% of the WS_2 crystallites in the range 20–30 Å, 37% in the range 30–40 Å, and 16% in the range 40–50 Å. Only 20% of the crystallites were beyond or below these sizes. For the sample with 2.5

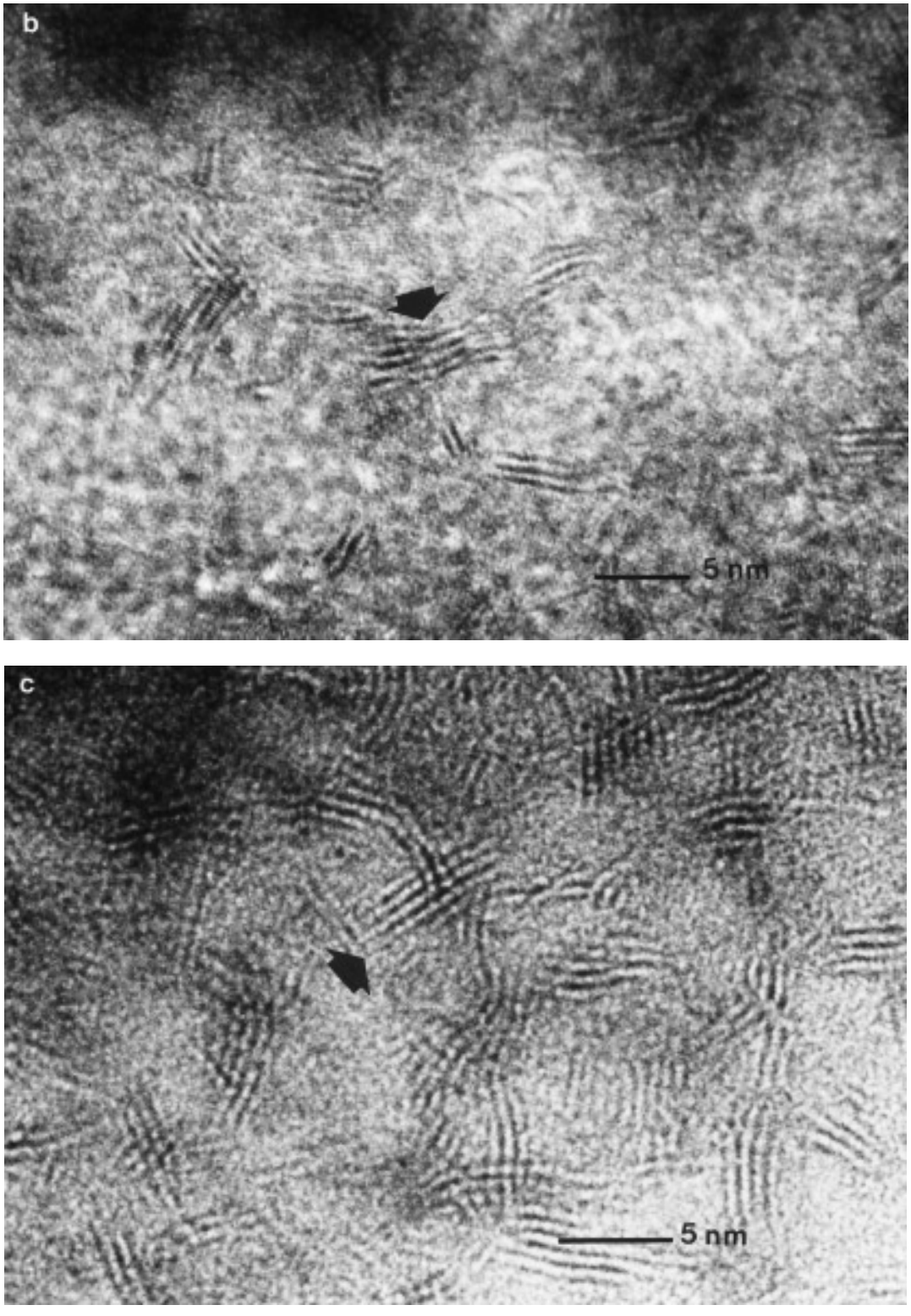

FIG. 9—*Continued*

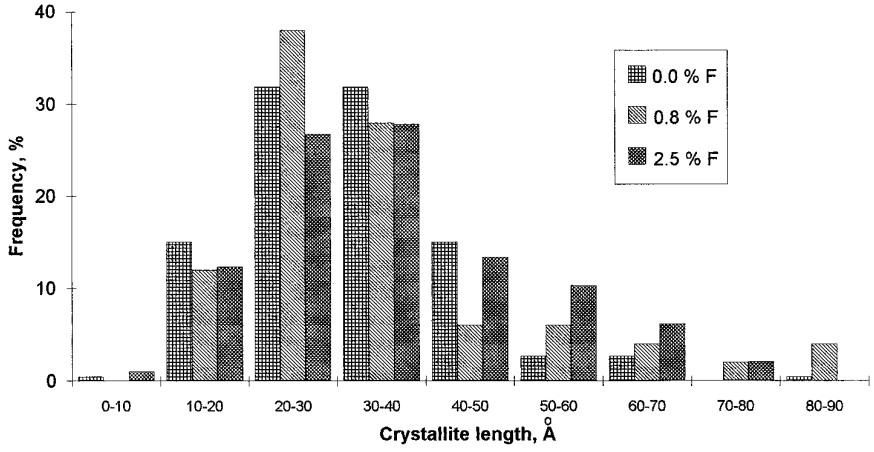

FIG. 10. Length distribution of the WS_2 crystallites observed in the T–NiW–F(x) catalysts.

wt% F^-, the distribution was shifted toward the longer sizes; 27% of the WS_2 crystallites were between 20 and 30 Å, and 22% between 40 and 50 Å.

The fact that only small changes in L are obtained with the addition of F^- may be due to the presence of the Ni promoter, which inhibits the growth of the crystallites in the lateral direction as a result of its interaction with the edge W atoms in the WS_2 crystallites to form the active NiWS sites.

For the fluoride-free sample the average number of layers was 3.0 whereas for the sample with 2.5 wt% F^- the average number of layers was 3.14. This small effect can be better appreciated by a detailed analysis of Fig. 11 where it is easier to observe the shift toward higher stacking with fluoride incorporation.

An interesting feature which was only observed in the catalyst with 0.8 wt% F^- was that in addition to the presence of the normal-size WS_2 structures, very large WS_2 structures were also found. These very large WS_2 structures are clearly not representative of typical WS_2 crystallites. Figure 12 shows an example of these structures in which excessive lateral growth was promoted. These very large WS_2 structures, which have not been reported previously, presented more than 20 layers and lengths of more than 50 nm. It is possible that these large structures were the result of local concentration gradients of the different species present in the catalyst, since it is well known that the interaction of the promoter located on the edge sites of the WS_2 crystallites prevents their lateral growth (16). Since these abnormally large crystallites are presumably larger than the pore dimensions, it would seem most likely that these structures originate from phases deposited on the outside of the catalyst particles. However, the frequency of appearance of these very large WS_2 structures was small compared to that of the normal-size WS_2 structures. These very large WS_2 structures, found in the sample with 0.8 wt% F^-, were not taken into account in plotting the crystallite size and stacking distributions.

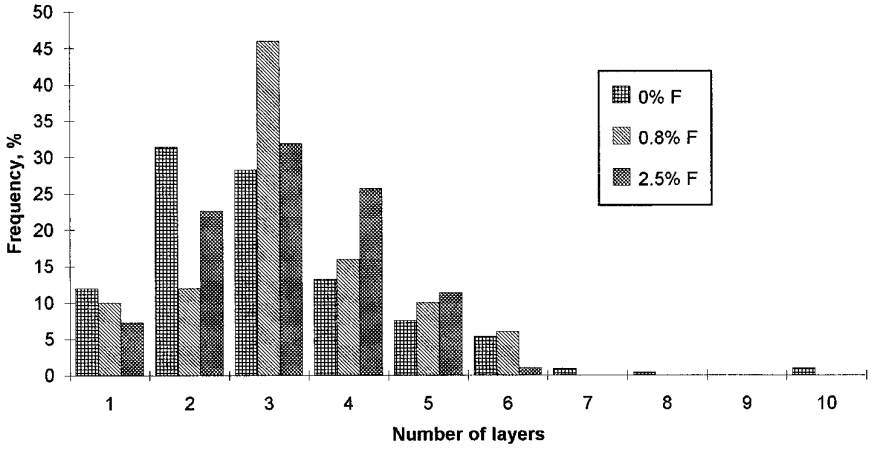

FIG. 11. Distribution of the number of layers of the WS_2 crystallites in the T–NiW–F(x) catalysts.

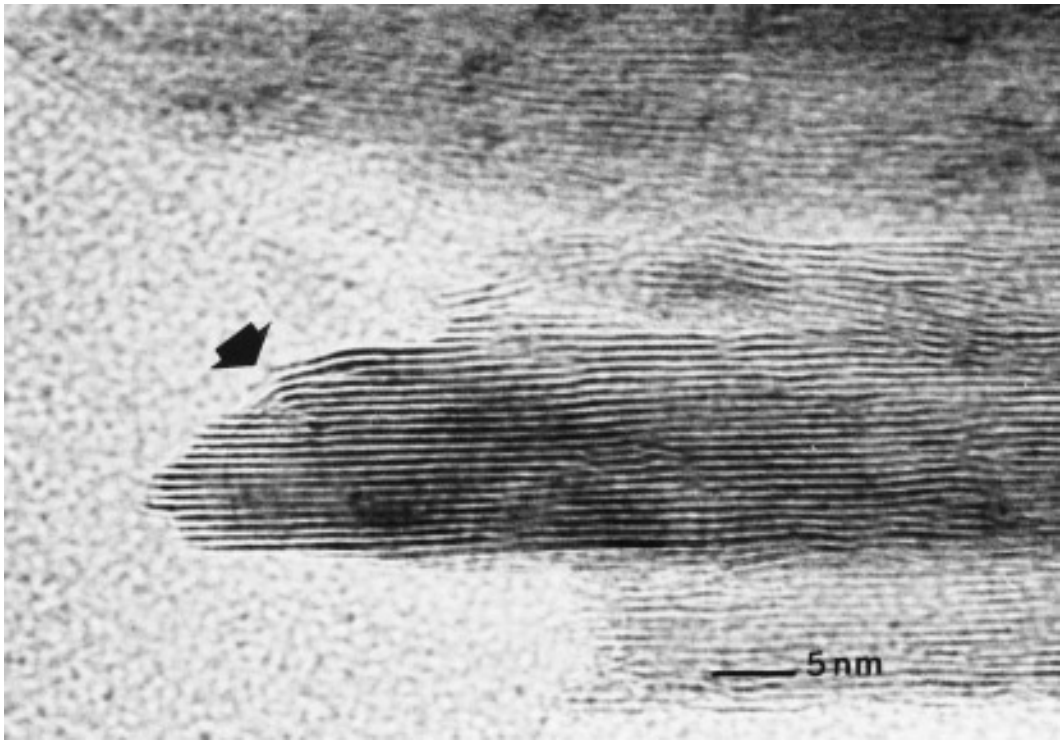

FIG. 12. Micrograph of one of the abnormally large WS_2 structures found in the T–NiW–F(0.8) catalyst sample.

An estimation of the total number of observed tungsten atoms, similar to the one done for the catalysts prepared with the oxisalt precursor, was performed with the T–NiW–F(x) samples. The results from such calculations are presented in Table 2, where one can see that in these samples, the incorporation of fluoride has almost no influence on the density of observed tungsten atoms in sulfided form, in the catalysts with 0, 0.8, and 2.5 wt% F^-. Since in these samples the tungsten loading was 2.8 tungsten atoms per square nanometer one may infer a good level of sulfidation. This result may be due to the fact that in this case the catalyst precursor has four sulfur atoms per atom of tungsten, and after the sulfidation procedure one obtains two sulfur atoms per atom of tungsten in the tungsten disulfide. The excess of sulfur in the precursor may also be the cause for the sulfur entities observed in the T–NiW–F(x) catalysts.

The drop in the number of observed tungsten atoms in the T–NiW–F(0.8) catalyst sample can be rationalized if one takes into account that in this sample some very large WS_2 structures were observed which, as mentioned before, were not taken into account for the statistics of WS_2 crystallites.

Which of the two catalyst precursors leads to a greater degree of sulfidation may be judged by comparing the total number of observed tungsten atoms per square nanometer in the fluoride-free samples. As expected, the density of observed tungsten atoms in the O–NiW–F(0) catalyst (W_t = 1.75) was lower than that of the T–NiW–F(0) sample (W_t = 2.33), suggesting a better sulfidation of the latter. Furthermore, in contrast with the oxisalt-prepared catalysts, in which the stacking of the WS_2 was low, in the T–NiW–F(x) the stacking of the WS_2 crystallites was higher, despite the fact that they had a lower tungsten loading. This increase in the stacking of the thiosalt-prepared catalysts may be related to the fact that in these catalysts the calcination step is skipped and therefore, the interaction of the tungsten species with the alumina support is not favored during the catalyst preparation process, leading to a greater possibility of an enhanced stacking of the WS_2 crystallites. This precursor salt effect appears quite clearly when the fluoride-free catalysts obtained by the two methods of preparation are compared (Figs. 1 and 9). The above results may be summarized by stating that fluoride incorporation in both methods of preparation increases the size of the WS_2 crystallites but has only a small influence on their average number of layers. In contrast, the change of precursor salt has an important influence on the stacking but little influence on the size of the WS_2 crystallites. Our results indicate that the size and architecture of the WS_2 crystallites is mainly governed by the tungsten–support interactions during the preparation procedure rather than by changes in the stabilization energy of the WS_2 nanocrystallites, which could be induced by the presence of the fluoride ions on the alumina surface. Also, fluoride incorporation in the T–NiW–F(x) catalysts appar-

TABLE 2

Average *N* and *L* Values and Total Observed W Atoms per Square Nanometer, for the Thiosalt-Prepared NiW/Al_2O_3-F(x) Catalysts

Fluoride content	N	σ_N[a]	L (nm)	σ_L[a]	Total observed W atoms/nm^2
0	3.00	0.15	3.17	0.52	2.33
0.8	3.22	0.13	3.53	0.30	1.97
2.5	3.14	0.12	3.51	0.38	2.28

[a] Standard deviation for number of layers (σ_N) and crystallite length (σ_L).

ently reduces the deposition of large thiosalt clusters on the alumina surface.

The quantitative estimates of the total number of observed tungsten atoms, which suggested an improvement in the sulfidation of the samples with fluoride loading, agree well with previously reported results in nonpromoted tungsten catalysts supported on alumina modified by fluoride (4, 5), in which the addition of fluoride promoted the formation of polytungstates and increased the reducibility of the catalyst oxidic precursors.

Although it is possible that the "unobserved" WS_2 structures will have an effect on the catalytic behavior of the samples prepared by both types of precursor salts, in our samples the majority of the structures are observed, especially in the samples prepared with thiosalt precursors and those prepared with oxisalt but with high fluoride loading.

Finally, the observed differences in the architecture in the WS_2 crystallites promoted either by a change in the precursor salt or by the incorporation of fluoride into the alumina support are likely to be reflected in differences in the hydrodesulfurization and hydrodenitrogenation activities of the two catalyst series. Work is in progress to test this last assumption.

CONCLUSIONS

An electron microscopy study of NiW/Al_2O_3–F(x) catalysts prepared using ammonium metatungstate and ammonium tetrathiotungstate as W precursors has been made.

From the observations of this study the following conclusions can be drawn:

For the two series of catalysts prepared via oxisalt and thiosalt impregnation, it is evident that, for the same F^- content, the thiosalt method, which promotes a smaller interaction between the W species and the alumina support, leads to higher stacking than the oxisalt method but to similar length of the WS_2 crystallites.

In both methods of catalyst preparation fluoride incorporation increases the length of WS_2 crystallites but has only a small effect on their stacking.

The thiosalt method of preparation leads to catalysts with an excess of sulfur distributed in a nonhomogeneous way.

For the catalysts prepared via the thiosalt method, fluoride incorporation favored the decomposition of large $(NH_4)_2WS_4$ crystals.

ACKNOWLEDGMENTS

Financial support from CICYT, Project PB87-0261 (Spain), CONACyT (Mexico), CSIC (Spain), and DGAPA (UNAM, Mexico) is gratefully acknowledged.

REFERENCES

1. Yang, S. H., and Satterfield, C. N., *Ind. Eng. Chem. Process Des. Dev.* **23,** 20 (1984).
2. Fierro, J. L. G., Cuevas, R., Ramírez, J., and López-Agudo, A., *Bull. Soc. Chim. Belg.* **100,** 945 (1991).
3. Payen, E., Hubaut, R., Kasztelan, S., Poulet, O., and Grimblot, J., *J. Catal.* **147,** 123 (1994).
4. Codero, R. L., Solis, J. R., Ramos, J. V. G., Patricio, A. B., and Agudo, A. L., *in* "New Frontiers in Catalysis" (A. Guczi, F. Solymosi, P. Tetenyi, Eds.), Proceedings, 10th International Congress on Catalysis, Part C, p. 1927. Akadémiai Kiadó, Budapest, and Elsevier, Amsterdam, 1993.
5. López-Agudo, A., Benitez Patricio, A., Ramírez Solis, J., and Vazquez, A., Abstract B-42 of the 13th North American Meeting of the Catalysis Society, Pittsburgh, PA, 1993.
6. Moon, S. H., and Song, C. J., Abstract B-52 of the 13th North American Meeting of the Catalysys Society, Pittsburgh, PA, 1993.
7. Benitez Patricio, A., Ph.D. Thesis, Universidad Complutense de Madrid, Madrid, Spain, 1992.
8. Zaikovski, L. M., Plyasova, V. A., Burmistrov, A. N., Startsev, A. N., and Yermakov, Yu. I., *Appl. Catal.* **11,** 15 (1984).
9. Breysse, M. *et al. Catal. Today* **4,** 39 (1988).
10. Papadopoulou, Ch., Lycourghiotis, A., Grange, P., and Delmon, B., *Appl. Catal.* **38,** 273 (1988).
11. Ramírez, J., Cuevas, R., López-Agudo, A., Mendioroz, S., and Fierro, J. L. G., *Appl. Catal.* **57,** 223 (1990).
12. Kasztelan, S., Toulhoat, H., Grimblot, J., and Bonelle, P., *Appl. Catal.* **13,** 127 (1984).
13. Toulhoat, H., and Kasztelan, S., *in* "Proceedings, 9th International Congress on Catalysis, Calgary, 1988," (M. J. Phillips and M. Ternan, Eds.), Vol. 1. Chem. Institute of Canada, Ottawa, 1988.
14. Breysse, M. *et al.*, *Catal. Today* **4,** 39 (1988).
15. Grimblot, J. *et al.*, *J. Electron Spectrosc. Relat. Phenom.* **52,** 485 (1990).
16. Ramírez, J., Fuentes, S., Diaz, G., Vrinat, M., Breysse, M., and Lacroix, M., *Appl. Catal.* **52,** 211 (1989).